Inhibitory Effect of Clay/Chitosan Nanocomposite against *Penicillium digitatum* on Citrus and Its Possible Mode of Action

Khamis Youssef [1,*] and Ayat F. Hashim [2]

[1]*Agricultural Research Center, Plant Pathology Research Institute, 9 Gamaa St., 12619 Giza ;* [2]*Food Industry and Nutrition Division, National Research Centre, 33 El Buhouth 12622 Giza, Egypt*

Abstract

Citrus postharvest diseases are commonly controlled by applying synthetic fungicides in packinghouses. Several limitations to pesticides have resulted in a considerable interest in developing alternative non-polluting control means. Clay/chitosan nanocomposite (CCNC) was prepared by an anion exchange reaction between chitosan and clay. The structure and morphology of CCNC was characterized by Fourier-transform infrared spectroscopy (FT-IR), X-ray diffraction (XRD), Transmission electron microscopy (TEM), Scanning electron microscopy (SEM) and energy-dispersive X-ray (EDX). FTIR data and XRD patterns indicate that chitosan was intercalated into the clay layers. TEM result also showed that the dark sheets of clay were dispersion in chitosan matrix. The surface morphology of CCNC in SEM micrograph showed a massive layered structure with some large flakes and some inter layer spaces. The EDX spectra of the prepared nanocomposite show key elements like C, O, Mg, Al and Si. The fungicidal activity of CCNC was tested against *Penicillium digitatum in vitro* and *in vivo*. A complete inhibition of *P. digitatum* was achieved at 20 μg mL^{-1} for clay/chitosan (1:0.5), clay/chitosan (1:1) and clay/chitosan (1:2). CCNC was tested *in vivo* for a direct and indirect action (induction of resistance) against green mold of oranges cv. Valencia late. The results showed that considering CCNC direct action a complete inhibition of green mold was observed, whereas a high reduction (70%) of rot was reported for clay/chitosan (1:2) used as a resistance inducer. The mode of action of CCNC on the pathogens was also demonstrated via the genotoxicity (degradation of *P. digitatum*-DNA) and SEM (severe collapse, malformation and irregular branching of hyphae). CCNC is economically interesting because it is easy to prepare and involves inexpensive alternative control means against green mold of citrus fruit.

Keywords: nanocomposite; *Penicillium digitatum*; chitosan; citrus; clay

1. Introduction

Citrus is a widely spread fruit crop in Egypt, and it is considered to be the most important fruit crop. During 2017, the total Egyptian production was 3013758 tonnes, and 166775 tonnes of Egyptian citrus have been exported (Faostat, 2017). In Egypt, climate is suitable to the production of citrus fruit especially oranges, which accounts for over half of the total fruit production; exported amount of the fresh and dried citrus fruit, especially oranges, reached 2.2% of the total worldwide exported amount. The economic losses due to fungal infection in fruits and vegetables during the postharvest chain are variable and not well documented. They usually reach anywhere from 30 to 50% and, on some occasions, decays can lead to total loss of the produce (Bautista-Baños, 2014).

Penicillium digitatum (Pers.:Fr.) Sacc. is the most severe postharvest fungal pathogen of citrus fruit agent of green mold, which may cause 60–80% of decay under ambient conditions (MoscosoRamírez *et al.,* 2013; Youssef *et al.,* 2014). Citrus postharvest diseases are frequently controlled globally by applying synthetic fungicides in packinghouses before fruit storage. However, the use of chemical fungicides is facing many constrains, including the development of pathogen resistance and the public concern related to health and environmental hazards. Those problems resulted in a significant interest in developing alternative safer control means (Fallanaj *et al.,* 2015; Youssef *et al.,* 2017).

Chitosan, β-(1,4)-2-amino-2-deoxy-D-glucose, is a natural versatile biopolymer derived by partially deacetylation of chitin, mainly as the structural component of the exoskeletons of crustaceans and insects, as well as in some fungal cell walls (Sanford, 2003). This polymer is among those naturally-occurring compounds that have potential in agriculture, especially for controlling plant diseases. Chitosan has been shown to be fungicidal against several fungal plant pathogens (Liu *et al.,* 2001; Rabea and Steurbaut, 2010). One of the most important attributes of chitosan is its fungistatic/fungicidal activity toward postharvest fungi at various concentrations (*Alternaria alternata, Colletotrichum gloeosporioides, Fusarium oxysporum, Rhizopus stolonifer, Penicillium spp., Botrytis cinerea, Neurospora crassa*) (Bautista-Banos *et al.,* 2006; Reglinski *et al.,* 2010).

Montmorillonite clay belongs to the smectite group, a diverse group of clay minerals with a 2:1-layer silicate structure that can expand and contract upon wetting and drying, composed of layers of two silica tetrahedral sheets surrounding a central alumina octahedral sheet (Abdeen and Salahuddin, 2013). In addition, the substantial harmlessness of montmorillonite makE it a promising

---

nanofiller to be broadly utilized in food industry (Xu *et al.,* 2018). Polymer-clay nanocomposites are a class of hybrid materials composed of organic polymer matrices and nanoscale organophilic clay fillers. When nanoclay is mixed with a polymer, three types of composites (tactoids, intercalation, and exfoliation) can be obtained (Xu *et al.*, 2006). For the most part, polymer/clay nanocomposites contain a natural organic/inorganic hybrid polymer network comprising platelet-shaped clay particles that have sizes in the order of a few nm thick and several hundred nm length. Due to clay particles high phase ratio and surface area, if suitably dispersed in the polymer matrix at a loading of 1–5 weight percent, instruct sole combinations of physical and chemical properties to make them attractive for films and coatings in a broad collection of industries (Han *et al.,* 2010).

The purpose of the present research was (i) to prepare and characterize clay/chitosan nanocomposite (CCNC), (ii) to evaluate the efficacy of CCNC *in vitro* against *P. digitatum*, iii) to assess the efficiency of CCNC against green mold under artificial infection on citrus fruit, and (iv) to evaluate their possible toxicity by using scanning electron microscopy (SEM) and DNA-binding assays.

2. Material and methods

Chitosan was purchased from Acros (Morris Plains, NJ, USA) with a degree of deacetylation and average MW of 85% and 100.000 Da, respectively. Natural montmorillonite (Cloisite®Na$^+$) was received from Southern Clay Products Inc (TX; USA). Acetic acid 99-100% was provided from Honeywell (Muskegon, MI, USA).

2.1. Preparation of CCNC

CCNC was prepared following the protocol of Han et al. (2010). In particular, aqueous solution of chitosan was prepared by dissolving desired weight ratio of chitosan powder in 100 ml of acetic acid solution (1%, v/v) and stirring for about 2 h. A 1 wt% clay suspension was also prepared by dispersing clay powder in distilled water and stirring for 12 h prior to use. The chitosan solution was then slowly added to the clay suspension at 60°C. During the mixing process, the weight ratio of clay to chitosan was (1:0.5, 1:1 and 1:2) in order to control the chitosan loading level in the clay layers. The reaction mixture was stirred for 2 h, separated by centrifugation and washed three times with distilled water. Then the nanocomposites were dried at 100°C for 12 h and well ground to power.

2.2. Characterization of CCNC

2.2.1. Fourier-transform infrared spectroscopy (FT-IR)

CCNC was analyzed by FT-IR spectroscopy as described by Youssef et al. (2017) with minor optimization. The CCNC solution was centrifuged at 25,000 ×g for 25 min and washed twice in deionized water to remove the unbound components. The purified samples and potassium bromide (KBr) were grounded to reduce the diameter size of particle to less than 5 mm. A small amount of sample mixed with the KBr powder then ground the mixture for 3-5 minutes. The powder was added to collar and put it together with the die into press to form pellet and subsequently analysed on a Jasco FT-IR 5300 spectrophotometer. The samples were directly placed in the zinc selenide crystal, and the spectrum was recorded in the transmittance mode.

2.2.2. X-ray diffraction (XRD)

Crystalline materials produce distinct x-ray diffraction (XRD) patterns that can be used for the identification of the phases present in a material. Current approaches use the entire background subtracted spectrum. XRD patterns of CCNC have been recorded using Panalytical Empyrean (PANalytical, Netherlands), using CuKα radiation α 1.5406 Å, and scanning rate 0.1$^°$ in the 2θ range from 20$^°$ to 70$^°$ and step time 1 s (Hashim *et al.,* 2019).

2.2.3. Transmission electron microscopy (TEM)

TEM imaging was performed as described by Youssef et al. (2017). In particular, 20 μl of diluted CCNC were placed on a film coated 200-mesh copper specimen grid for 10 min. The grid was stained with one drop of phosphotungstic acid (3%) and left to dry for 3 min. The coated grid was dried and examined under the TEM microscope (Philips, CM12), and CCNC was observed by operating at 120 kV.

2.2.4. Scanning Electron Microscopy (SEM)

The surface morphology and shape of the optimized CCNC was studied by SEM (quanta FEG 250, Czech Republic). Samples were coated with gold to avoid charging of the surface. Then, the samples were examined under SEM at HV 25.0 kV, equipped with an energy-dispersive X-ray spectrometer (EDX).

2.3. Antifungal Activity of CCNC against P. digitatum in vitro

Agar plugs (5 mm Ө) from the growing edge of one-week-old cultures of *P. digitatum* were placed in the center of potato dextrose agar (PDA) Petri dishes amended with 250 mg L^{-1} of ampicillin and 250 mg L^{-1} of streptomycin to avoid contamination. For each PDA plate, three holes (5 mm Ө) at the corner of each plate were inoculated with 20 μl of CCNC. Five concentrations (5, 10, 20, 40 and 60 μg mL^{-1}) were used. PDA plates with sterilized distilled water were included as control. Five Petri dishes were utilized as replicates for each treatment, and the entire experiment was repeated twice. Colony diameter (mm) was measured after four days of incubation at 24 ± 1 °C. The percentage of reduction in colony diameter (CD) was calculated according to Salem et al. (2016) as follows:

CD (reduction, %) = (dc – dt) /dc× 100

Where: dc = average colony diameter in control plates
dt = average colony diameter of linear growth in treatment plates

2.4. Antifungal activity of CCNC against green mold in vivo

2.4.1. Fruit samples and Conidial Suspension:

Mature *Citrus sinensis* (L. Obseck) fruit cv. Valencia late were harvested from a private orchard in Cairo-Alexandria (desert road), selected for uniformity of size and absence of symptoms of any disorders. Fruits were surface sterilized with a 2% sodium hypochlorite for two min, washed with tap water and air-dried at room temperature. The fruits were divided randomly into two lots to perform the two sets of experiments (direct and indirect activity of CCNC against green mold). *P. digitatum* isolate code MF568039 (Hussien *et al.,* 2018) was grown on PDA plates at 24 ± 1°C in the dark to produce fungal inoculum. The conidial suspension was

prepared according to the standard protocol to obtain a final concentration of 10^4 conidia ml^{-1} (Youssef *et al.,* 2010).

2.4.2. Direct Antifungal Activity of CCNC

Oranges were wounded (5 mm depth × 3 mm wide) with a sterile nail-head at two equidistant points in the equatorial zone. A 20 µl aliquot of CCNC solution (20 µg ml^{-1}) was applied into each wound. After 2 h, 10 µl of 10^4 conidia ml^{-1} *P. digitatum* suspension was inoculated into the same wound site. Oranges treated with distilled sterile water and inoculated with the same concentration of the pathogen were included as control. Each treatment was replicated three times, and each replicate consisted of four oranges with two wounds each. Treated fruits were placed in plastic boxes covered with bags to maintain high humidity (90-95%) and incubated at 24±1 °C for one week. The incidence of decay (infected wounds, %) and disease severity (lesion diameter, mm) were recorded. The whole experiment was performed twice.

2.4.3. Indirect Antifungal Activity of CCNC

Oranges were wounded once with a sterile nail-head along the equatorial axis. For each treatment, a 20 µl aliquot of a CCNC solution (20 µg ml^{-1}) was applied into each wound. After 24 h of incubation at 24 ± 1 °C under high relative humidity (90-95%), another wound was made approximately 5 mm apart from the previous one. This wound was inoculated with 10 µl of 10^4 conidia ml^{-1} suspension of *P. digitatum* (Fallanaj *et al.,* 2016). Oranges, treated in the first wound with sterile distilled water and then inoculated with the pathogen conidial suspension in the other one, were included as control. Treatments and replicates were the same as described above. Fruit were incubated and the decay incidence and severity were recorded as described for direct antifungal activity. The entire experiment was performed twice.

For both *in vitro* and *in vivo* experiments, individual chitosan, clay, acetic acid and tecto 50% SC at 9 ml/L (Thiabendazole 50%, Syngenta Agro Egypt) were used for comparison.

2.5. The mode of action of CCNC

2.5.1. Scanning electron microscopy (SEM)

Plugs of *P. digitatum* (6 mm Ө) were cut from cultures grown for four days on PDA amended or not with CCNC at 20 µg ml^{-1} and placed in vials containing 3% glutaraldehyde and 2 % paraformaldehyde in 0.1 M sodium cacodylate buffer (pH 7.2) at 4 °C. Samples were kept in this solution overnight for fixation and then washed three times with 0.1 M sodium cacodylate buffer (pH 7.2) for 10 min. Then, the samples were washed three times, for duration of ten minutes each, using different ethanol series (30, 50, 70, 90 and 100%). Samples were critical point dried with CO_2 created with gold and observed in Quanta FEG 250, Czech Republic (Simionato *et al.,* 2017).

2.5.2. Fungal Genomic DNA Binding/Degradation Assay

Total genomic DNA from *P. digitatum* was extracted following the methods of Moslem et al. (2010). After extraction, 10 µl of DNA was treated with CCNC (5 and 20 µg ml^{-1}) for a period of 2 h at 37 °C. The products resulting from interactions of the nanocomposite with DNA were separated by 1.5% (w/v) agarose gel containing 0.05 µg ml^{-1} ethidium bromide, to check the quality of the DNA. A charge-coupled device camera imaging system and UVI soft analysis (Gel Documentation and Analysis Systems, Uvitec, Cambridge, UK) were used to capture the image (Abd-Elsalam *et al.,* 2018).

2.6. Statistical Analysis

Percentage data were arcsine transformed before analyses to normalize variance. Data were processed statistically using Statistica 6.0 software (Stat Soft Inc., Tulsa, Oklahoma, USA). Mean values of treatments were compared using Duncan's multiple range test (DMRT) and judged at $P \leq 0.05$ level.

3. Results and Discussion

3.1. Preparation of CCNC

CCNC was prepared by an ion exchange process between oligomeric chitosan and Na^+ montmorillonite. The nanocomposites were rapidly prepared within 2 h, due to the high affinity between the chitosan and the clay host. Previous studies have confirmed a great diffusion of montmorillonite in chitosan polymer through the intercalation of cationic chains into montmorillonite interlayers, which grants the resulting nanocomposites with improved mechanical and barrier properties (Darder *et al.,* 2003; Xu *et al.,* 2018). The composites were ordinarily joined through adsorption, gelation, or intercalation due to of the electrostatic cooperation among chitosan and clay (Kumar *et al.,* 2019).

3.2. FT-IR measurements

FT-IR proved to be an appropriate technique to study polymer-clay interaction (Fig. 1). Clay spectrum showed the characteristic absorption bands at 3365 cm^{-1} due to – OH stretching band for absorbed water. The band at 3626 cm^{-1} was due to AOH band stretch for Al-OH. The overlaid absorption peak at 1624 cm^{-1} might be attributed to OH bending mode of absorbed water. The characteristic peaks at 1120 and 983 cm^{-1} were due to SiAO stretching (out of plane) and Si-O stretching (in-plane) vibration for layered silicate, respectively. Peaks at 903, 791, and 679 cm^{-1} might be attributed to AlAlOH, AlFeOH, and AlMgOH bending vibrations, respectively. FT-IR spectrum of chitosan showed peaks at 3346, 2867, 1661, 1587, 1418, 1132 and 1077 cm^{-1}, which were due to the asymmetric and symmetric stretching of methylene ($-CH_2$) groups, amide I, amide II, amide III,C-O-C stretching vibration and C-O stretching vibration respectively.

In the formed chitosan clay nanocomposite in 2:1 ratio, NH_3^+ groups of chitosan interacted electrostatically with the negatively charged sites of the clay; as such, the frequency of vibrational bands at 1587 cm^{-1}in the pure chitosan was shifted toward a lower value (1561 cm^{-1}). In the same context, Han et al. (2010) showed a shift in frequency of vibrational bands at 1554 cm^{-1} in the starting chitosan toward lower frequency values depending on the chitosan loading level. The intensity of this absorption was highly decreased due to the electrostatic interaction between cationic chitosan and anionic clay (Abd El-Kader *et al.,* 2015). The amide I band at 1661 cm^{-1} of chitosan may overlap with δHOH bending vibration band at 1624 cm^{-1} of the water molecule associated to the starting clay

as expected for the biopolymers with high water retention capability (Abd El-Kader *et al.,* 2015).
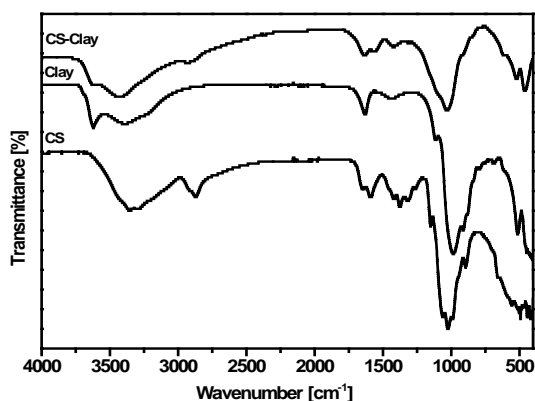
Figure 1. FT-IR spectra of synthesized clay/chitosan nanocomposite.

3.3. XRD analysis

The XRD analysis was used to study the crystallinity and the structural changes of the nanocomposite in the range of 2–70° as shown in (Fig. 2). The XRD pattern of clay presented a distinctive diffraction peak around 7° that corresponds to a d001 spacing (Giannakas *et al.,* 2014). Characteristic peaks of chitosan at around $2\theta = 10^{o}$, 20° and 23° were revealed in harmony with previous publications (Lavorgna *et al.,* 2010; Taghinezhad and Ebadollahi 2017). The peak at 10° shows a hydrated crystallite structure due to the water molecules integration in the crystal lattice. The peak at 18° is recognized to the regular crystal lattice of chitosan (Kittur *et al.,* 2003), whereas the broaden peak around 23° indicates an amorphous structure of chitosan (Rhim *et al.,* 2006; Lavorgna *et al.,* 2010). The XRD ranging up to $2\theta \approx 10$ to 25° shared by both chitosan and clay was quite different than that observed for XRD of both the two starting materials, indicating the occurred complexation between chitosan and the clay. It is obvious that addition of clay causes a decrease in the crystallinity of chitosan (Giannakas *et al.,* 2014). Both results of XRD and FT-IR supported each other indicating chitosan complexion with clay.
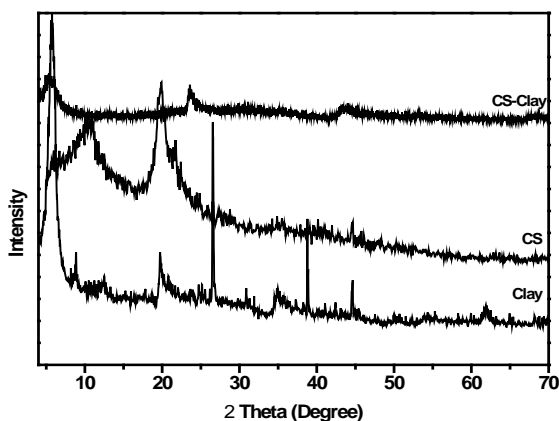
Figure 2. X-ray diffraction pattern of synthesized clay/chitosan nanocomposite.

3.4. Morphological observation by TEM and SEM

The morphology of the prepared CCNC was investigated by TEM and SEM (Fig. 3). There were several single silicate layers, as well as aggregates of silicate layers, dispersed in the polymer matrix. SEM micrograph displayed good and random dispersion of clay within chitosan matrix. From visual analysis of SEM images, a uniform appearance with small irregularities and bumps was noticed. It was also clear that the surface of MMT had an aggregated and foliated appearance due to the presence of the layered structure. The EDX spectra of the prepared CCNC showed key elements like C, O, Mg, Al and Si (Fig. 4). It was observed intercalated, stacked, and partially exfoliated structures of Chitosan/Montmorillonite-K10 nanocomposites Films according to XRD diffraction patterns and TEM observations. Moreover, an interaction between polymer matrix and MMMTK10 was observed from SEM images (Kasirga *et al.,* 2012).
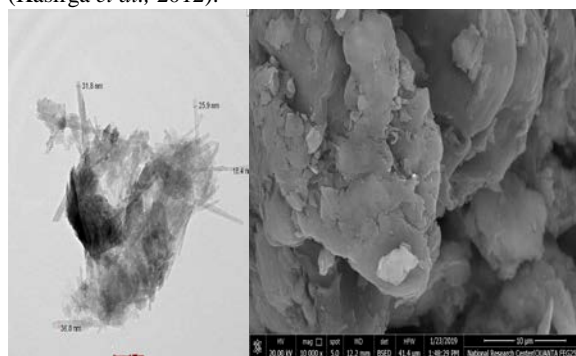
Figure 3. TEM and SEM micrograph of synthesized clay/chitosan nanocomposite.
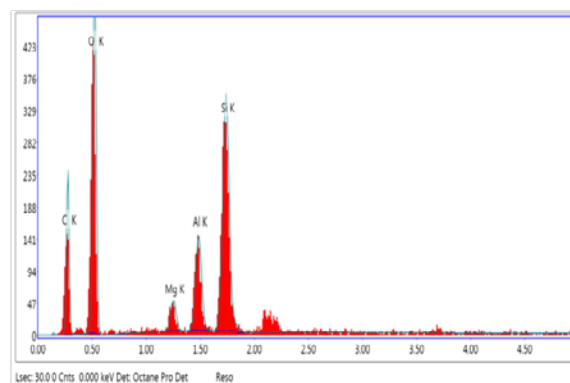
Figure 4. EDX micrograph of synthesized clay/chitosan nanocomposite.

3.5. Antifungal Activity Of CCNC Against P. Digitatum in Vitro

After 7 days of incubation, a complete inhibition of *P. digitatum* was achieved at 20 μg ml^{-1} for clay/chitosan (1:0.5), clay/chitosan (1:1) and clay/chitosan (1:2). At 10 μg ml^{-1}, the percentage of reduction of colony diameter was 73, 75 and 90% for clay/chitosan (1:0.5), clay/chitosan (1:1) and clay/chitosan (1:2), respectively, whereas a complete inhibition was observed at 60 μg ml^{-1} for chitosan and clay as standalone treatments. *P. digitatum* growth was completely inhibited by thiabendazole fungicide at all concentrations used, while acetic acid inhibited the pathogen growth at 20 μg ml^{-1} (Fig. 5 and 6). Similarly, chitosan NPs showed the

maximum growth inhibitory effects on *in vitro* mycelial growth of *Trametes versicolor* and *Tyromyces palustris* at 0.1% concentration (Suhartono, 2015). The mode of action by which chitosan affects the growth of fungi may be due to its ability to interfere with the negatively charged residues of macro-molecules exposed on fungal surfaces forming polyelectrolytic complexes, and affecting membrane permeability as well as causing leakage of intracellular electrolytes and proteinaceous constituents (Suhartono, 2015). Chitosan possesses a natural antifungal role by which it increases the permeability of the outer and inner membranes, thus disrupting bacterial cell integrity with the release of cellular metabolites, and finally chelation of trace metals inhibiting enzyme activities (Liu *et al.,* 2004). Chitosan/clay nanocomposites showed also a synergistic effect against *Escherichia coli* and *Staphylococcus aureus* (Han *et al.,* 2010).
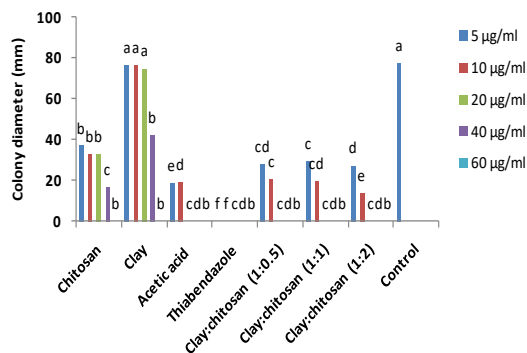
Figure 5. Effect of different concentrations of clay/chitosan nanocomposite on colony diameter (mm) of *P. digitatum* after four days incubation at 24±1°C on PDA. PDA amended with water was utilized as control. Chitosan, clay, acetic acid and thiabendazole were included for comparison. Statistical analysis was performed within each column. Values marked with the same letters are not statistically different according to posthoc test DMRT at p ≤ 0.05.
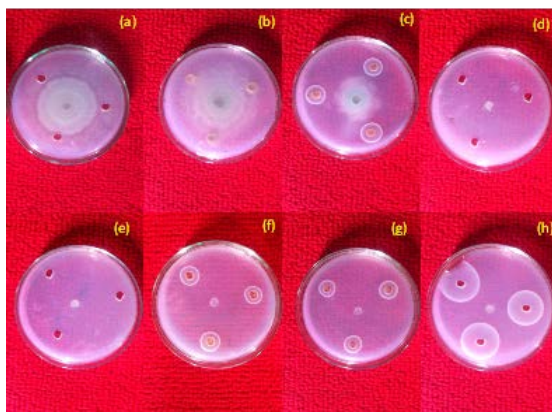
Figure 6. Effect of different concentrations of CCNC on colony diameter of *P. digitatum* after four days incubation at 24±1°C on PDA. A. control; B. clay; C. chitosan; D. acetic acid; E. thiabendazole; F. CCNC 1:0.5; G. CCNC 1:1; H. CCNC 1:2.

3.6. Antifungal Activity Of CCNC Against Green Mold In Vivo

In assays evaluating the direct action, decay incidence was 100, 83.3 and 50% for water control, clay and acetic acid, respectively (Fig. 7), while no decay incidence was observed for the remaining treatments. In the case of indirect action (in which compound and pathogen were

added into separate wounds), decay incidence was 100, 66.6, 100, 41.6, 25, 41.6, 33.3 and 33.3 for control, chitosan, clay, acetic acid, thiabendazole, clay:cs,(1:0.5), clay:cs(1:1) and clay:cs (1:2), respectively (Fig. 7). Our results were in agreement with Xu et al. (2018) who concluded that chitosan/montmorillonite demonstrated the most significant and extended impact as antifungal agent to decrease the tangerine decay percentage during storage.
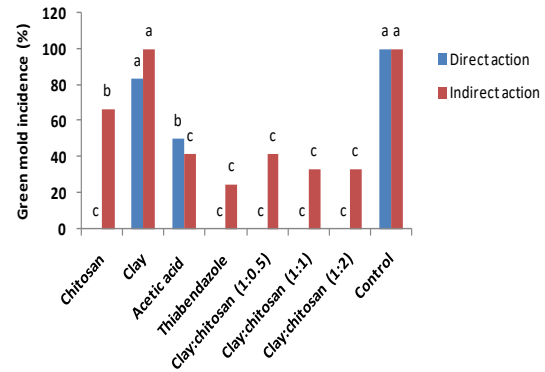
Figure 7. Decay incidence (%) of green mold after seven days of shelf-life at 24±1°C and high RH on "Valencia late" oranges treated with 20 µg/ml of clay/chitosan nanocomposite. Statistical analysis was performed within each column. Values marked with the same letters are not statistically different according to posthoc test DMRT at p ≤ 0.05. Direct action: the pathogen and clay/chitosan nanocomposite were applied into the same wound; indirect action: the pathogen and clay/chitosan nanocomposite were applied into separated wounds.

In assays evaluating the direct action, lesion diameter was completely inhibited by chitosan, thiabendazole, clay/chitosan (1:0.5), clay/chitosan (1:1) and clay/chitosan (1:2), whereas no complete inhibition of green mold was observed for clay or acetic acid. In case of indirect action, the reduction was 47, 50, 51 and 70% for chitosan, clay/chitosan (1:0.5), clay/chitosan (1:1) and clay/chitosan (1:2), respectively (Fig. 8).

Chitosan NPs were effective elicitors of host resistance to many plant pathogens infections (Pichyangkura and Chatchawan, 2015). Other GRAS compounds such as salts were used on citrus to control postharvest diseases such as sodium carbonate and bicarbonate. The ability to such salts was comprehensively investigated to induce natural resistance in oranges fruit including enzyme activity, gene expression levels, phytoalexin and sugar contents (Youssef *et al.*, 2014; Youssef *et al.*, 2015).

Novel chitosan/Ag/ZnO (CTS/Ag/ZnO) blend films were prepared and evaluated as antimicrobial agent (Li *et al.*, 2010). Their results revealed that ZnO and Ag nanoparticles had a uniform distribution within chitosan polymer; the produced blend had excellent antimicrobial activities against many bacterial, fungal, and yeast strains with higher antimicrobial activities than chitosan alone. In particular, Ag-chitosan nanocomposites might be proposed as efficient fungicidal agents for entire inhibition of *B. cinerea*, and grey mold prevention on strawberries.

Developing chitosan-layered silicate nanocomposites by inserting chitosan chains into interlayers of silicate can improve its mechanical properties. In recent years, polymer nanocomposites have received considerable interest because of their superior thermal and mechanical properties, as compared with the polymer itself (Kumar *et*

al., 2003). The obtained results herein suggest that clay would improve the protection function of chitosan polymer.
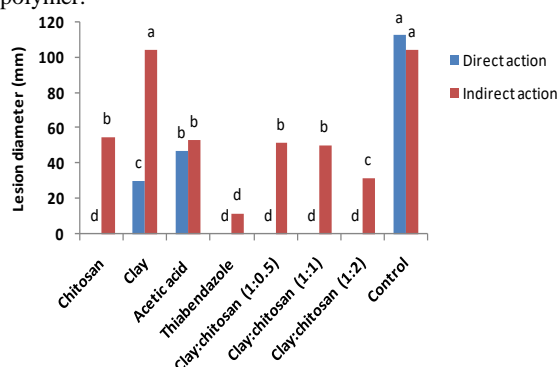
Figure 8. Lesion diameter (mm) of *P. digitatum* after seven days of shelf-life at 24±1°C and high RH on "Valencia late" oranges treated with 20 µg/ml of clay/chitosan nanocomposite. Statistical analysis was performed within each column. Values marked with the same letters are not statistically different according to posthoc test DMRT at p ≤ 0.05. Direct action: the pathogen and clay/chitosan nanocomposite were applied into the same wound; indirect action: the pathogen and clay/chitosan nanocomposite were applied into separated wounds.

3.7. Scanning Electron Microscopy

On the control samples SEM demonstrated a normal morphology, and linearly shaped and the apical hyphae were tapered with a smooth surface (Fig. 9A). Treatment by CCNC at 20 µg ml^{-1} caused severe collapse, malformation and irregular branching of hyphae in the apical part (Fig. 9B). The microscopic observation of *Rhizoctonia solani* hyphae exposed to chitosan nanocomposite showed severe damage resulting in the separation of layers of hyphal wall and collapse of fungal hyphae (Abd-Elsalam *et al.,* 2018). Nevertheless, much work has to be done regarding the mode of action of chitosan-based nanomaterials against plant pathogens (El Hadrami *et al.,* 2010).
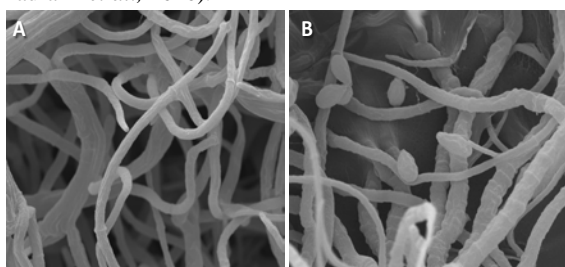
Figure 9. SEM of *P. digitatum* mycelia after 6 days of incubation at 24±1°C. A. Normal mycelium and free and linearly shaped hyphae (control); B. severely collapsed mycelium (treated with CCNC1:2). In the magnitude of 3000x (bar 20µm).

3.8. Fungal genomic DNA binding/degradation assay

CCNC was incubated with *P. digitatum* DNA to evaluate DNA binding as a possible molecular basis for their antifungal activities. The genotoxicity exhibited by CCNC was demonstrated by degradation of *P. digitatum* DNA at concentration 20 µg ml^{-1}. Control DNA exhibited one major characteristic band of unaffected/intact genomic DNA (Fig. 10). Chitosan-based nanocomposite treatment was effective to prevent amplification of PCR products. Oxidative damage can cause chemical degradation of DNA, which leads to PCR amplification failure when insufficient copies of DNA are present in the reaction (Abd-Elsalam *et al.,* 2018). Another important mechanism involves penetration of the chitosan oligomer into the cells of microorganisms, which inhibits the growth of cells by preventing the transcription of DNA into mRNA (Hernández-Lauzardo *et al.,* 2011).
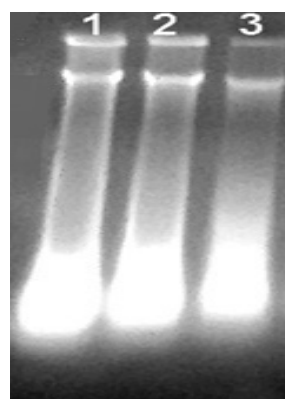
Figure 10. Agarose gel electrophoresis pattern of the fungal genomic DNA treated and untreated with CCNC1:2. Lane 1: DNA for untreated *P. digitatum*, Lane 2: *P. digitatum* treated with 5 µg CCNC, Lane 3: *P. digitatum* treated with 20 µg CCNC.

4. Conclusion

New strategies are needed with the serious goal of controlling green mold of citrus caused by *P. digitatum* with no fungicide residues. Clay/chitosan nanocomposite (CCNC) is economically interesting since it is easy to synthetize and low-cost chemical materials are needed. The chance to integrate at nanometric level clays and chitosan appears as an attractive method to change a portion of the properties of this polysaccharide including its mechanical and thermal behaviour, solubility and antifungal activity. CCNC seems to be an excellent alternative control means against green mold of citrus fruit.

Acknowledgement

References

Abd El-Kader FH, Shehap AM, Bakr AA and Hussein OT. 2015. Characterization of clay/chitosan nanocomposites and their use for adsorption on Mn(II) from aqueous solution. *Int J Sci Engin Appl,* **4**:174-185

Abdeen R and Salahuddin N. 2013. Modified chitosan-clay nanocomposite as a drug delivery system intercalation and i*n vitro* release of ibuprofen. *J Chem,* **2013**: 1-9

Abd-Elsalam KA, Vasil'kov AYu, Said-Galiev EE, Rubina MS, Khokhlov AR, Naumkin AV, Shtykova EV and Alghuthaymi MA. 2018. Bimetallic blends and chitosan nanocomposites: novel antifungal agents against cotton seedling damping-off. *Eur J Plant Pathol,* **151**:57–72

Bautista-Banos S, Hernandez-Lauzardo AN, Velazquez-Del Valle MG, Hernandez-Lopez M, Ait Barka E, Bosquez-Molina E and Wilson CL. 2006. Chitosan as a potential compound to control pre and postharvest diseases on horticultural Commodities. *Crop Prot,* **25**:108-118

Bautista-Baños S. 2014. Postharvest Decay: Control Strategies. Elsevier Inc, 1-383

Darder M, Montserrat CA, Ruizhitzky E. 2003. Biopolymer−clay nanocomposites based on chitosan intercalated in montmorillonite. *Chem Mater*, **15**:3774–3780

El Hadrami A, Adam LR, El Hadrami I and Daayf F. 2010. Chitosan in plant protection. *Marine Drugs* **8**:968–987

Fallanaj F, Sanzani SM, Youssef K, Zavanella C, Salerno MG, Ippolito A. 2015. A new perspective in controlling postharvest citrus rots: The use of electrolyzed water. *Acta Hort,* **1065**:1599-1606.

Fallanaj F, Ippolito A, Ligorio A, Garganese F, Zavanella C and Sanzani SM. 2016. Electrolyzed sodium bicarbonate inhibits *Penicillium digitatum* and induces defence responses against green mould in citrus fruit. *Postharvest Biol Technol*, **115**:18–29

FAOSTAT data: http://www.fao.org/faostat/en/#data/QC (Accessed 03 July 2019)

Giannakas A, Grigoriadi K, Leontiou A, Barkoula N and Ladavos A. 2014. Preparation, characterization, mechanical and barrier properties investigation of chitosan-clay nanocomposites. *Carbohydr Polym*, **108**:103-111

Han YS, Lee SH, Choi KH and Park I. 2010. Preparation and characterization of chitosan–clay nanocomposites with antimicrobial activity. *J Phys Chem Solids,* **71**: 467

Hashim AF, Youssef K and Abd-Elsalam KA. 2019. Ecofriendly nanomaterials for controlling gray mold of table grapes and maintaining postharvest quality. *Eur J Plant Pathol*, **154**:377–388

Hernández-Lauzardo A, Velázquez M and Guerra-Sánchez M. 2011. Current status of action mode and effect of chitosan against phytopathogens fungi. *Afri J Microbiol Res*, **5**:4243–4247

Hussien A, Ahmed Y, Al-Essawy AH and Youssef K. 2018. Evaluation of different salt-amended electrolysed water to control postharvest moulds of citrus. *Trop Plant Pathol,* **43**:10-20.

Kasirga Y, Oral A and Caner C. 2012. Preparation and characterization of chitosan/ montmorillonite-K10 nanocomposites films for food packaging applications. *Polym Comp,* **33**:1874-1882

Kittur FS, Vishu Kumar AB and Tharanathan RN. 2003. Low molecular weight chitosans--preparation by depolymerization with *Aspergillus niger* pectinase, and characterization. *Carbohydr Res,* **338**:1283-1290

Kumar S, Jog JP and Natarajan U. 2003. Preparation and characterization of poly(methyl methacrylate)–clay nanocomposites via melt intercalation: the effect of organoclay on the structure and thermal properties. *J Appl Polym Sci,* **89**:1186–1194.

Kumar S, Ye F, Dobretsov S and Dutta J. 2019. Chitosan nanocomposite coatings for food, paints, and water treatment applications. *Appl Sci,* **9**:1-27

Lavorgna M, Piscitelli F, Mangiacapra P and Buonocore GG. 2010. Study of the combined effect of both clay and glycerol plasticizer on the properties of chitosan films. *Carbohydr Polym,* **82**:291-298

Li LH, Deng JC, Deng HR, Liu ZL and Li XL. 2010. Preparation, characterization and antimicrobial activities of chitosan/Ag/ZnO blend films. *Chem Eng J,* **160**:378–82

Liu HY, Du X and Wang LS. 2004. Chitosan kills bacteria through cell membrane damage. *Int J Food Microbiol,* **95**:147-155

Liu XF, Guan YL, Yang DZ, Li Z and Yao KD. 2001. Antibacterial action of chitosan and carboxymethylated chitosan. *J Appl PolymSci,* **79**:1324–1335

Moscoso-Ramírez PA, Montesinos-Herrero C and Palou L. 2013. Characterization of postharvest treatments with sodium methylparaben to control citrus green and blue molds. *Postharvest Biol Technol*, **77**:128-137

Moslem MA, Abd-Elsalam KA, Bahkali AH and Yassin MA. 2010. First morpho-molecular identification of *Penicillium griseofulvum* and *P. aurantiogriseum* toxicogenic isolates associated with blue mold on apple. *Food-Borne Pathogen Dis,* **7**: 857–861

Pichyangkura R and Chatchawan S. 2015. Bio stimulant activity of chitosan in horticulture. *SciHortic,* **195**:49-65

Rabea EI and Steurbaut W. 2010. Chemically modified chitosans as antimicrobial agents against some plant pathogenic bacteria and fungi. *Plant Prot Sci,* **4**:149–158

Reglinski T, Elmer PAG, Taylor JT, Wood PN and Hoyte SM. 2010. Inhibition of Botrytis cinerea growth and suppression of botrytis bunch rot in grapes using chitosan. *Plant Pathol,* **59**:882–890

Rhim JW, Hong SI, Park HM and Ng PK. 2006. Preparation and characterization of chitosan-based nanocomposite films with antimicrobial activity. *J Agric Food Chem,* **54**:5814-22

Salem EA, Youssef K, Sanzani SM. 2016. Evaluation of alternative means to control postharvest Rhizopus rot of peaches. *Sci. Hort,* **198**:86–90.

Sanford PA. 2003. Commercial sources of chitin and chitosan and their utilization. In: Varum KM, Domard A, SmidsrØd O (eds) Advances in Chitin Science, vol 6. NTNU, Trondheim, pp 35–42

Simionato AS, Navarro MOP, de Jesus MLA, Barazetti AR, da Silva CS, Simões GC, Balbi-Peña MI, de Mello JCP, Panagio LA, de Almeida RSC and Andrade G de Oliveira AG. 2017. The Effect of phenazine-1-carboxylic acid on mycelial growth of *Botrytis cinerea* produced by *Pseudomonas aeruginosa* LV strain. *Front Microbiol,* **8**:1102

Suhartono D. 2015. Preparation of chitosan material and its antifungal activity for bamboo. *Int J Sci Res,* **6**:1586-1590

Taghinezhad E and Ebadollahi A. 2017. Potential application of chitosan-clay coating on some quality properties of lemon during storage. *Agric Eng Int,* **19**:189-194

Xu D, Qin H and Ren D. 2018. Prolonged preservation of tangerine fruits using chitosan/montmorillonite composite coating. *Postharvest Biol Technol,* **143**: 50–57

Xu Y, Ren X and Hanna MA. 2006. Chitosan/Clay Nanocomposite Film Preparation and Characterization. *J Appl Polym Sci,* **99**:1684–1691

Youssef K, Hashim AF, Margarita R, Alghuthaymi MA and Abd-Elsalam KA. 2017. Antifungal efficacy of chemically-produced copper nanoparticles against *Penicillium digitatum* and *Fusarium solani* on citrus fruit. *The Philip Agric Sci,* **100**:69-78

Youssef K, Sanzani SM, Ligorio A, Ippolito A and Terry LA. 2014. Sodium carbonate and bicarbonate treatments induce resistance to postharvest green mould on citrus fruit. *Postharvest Biol Technol,* **87**:61–69

Youssef K, Ahmed Y, Ligorio A, D'Onghia AM, Nigro F, Ippolito A. 2010. First report of *Penicillium ulaiense* as a postharvest pathogen of orange fruit in Egypt. *Plant Pathol,* **59**(6):1174.

Youssef K, Sanzani SM, Ligorio A, Fallanaj F, Nigro, F, Ippolito A. 2015. Biochemical and transcriptomic changes associated with induced resistance in citrus fruits treated with sodium salts. *Acta Hortic,* **1065**:1627–1632